# Catalysis Science & Technology



PAPER

View Article Online
View Journal | View Issue



Cite this: Catal. Sci. Technol., 2024, **14**, 4622

Received 25th March 2024, Accepted 29th June 2024

DOI: 10.1039/d4cy00404c

rsc.li/catalysis

# Selective deoxygenation of polar polymers using metal supported on TiO<sub>2</sub> nanotubes†

Dai-Phat Bui, D Laura A. Gomez, Ismael Alalq, Luis Trevisi, Ana Carolina Jerdy, Han K. Chau, Lance L. Lobban and Steven P. Crossley \*\*

Polar polymers such as poly(vinyl alcohol-co-ethylene) (EVOH) serve as excellent oxygen barriers in multilayered polymer films. However, their presence creates significant challenges for subsequent recycling. Melting and thermal degradation leave behind small domains of immiscible phases that render the final material less valuable. Here, we report a strategy to selectively remove OH groups from the EVOH polymer while preserving the polymer's hydrocarbon backbone. Pd supported on TiO<sub>2</sub> nanotubes exhibits excellent activity and selectivity for C–O bond scission and hydrogenation. This is evidenced in our study, which utilizes both the model compound 2,5-hexanediol (a small surrogate for polyols) and EVOH. The Lewis-acid sites generated on the TiO<sub>2</sub> surface, coupled with hydrogen dissociation on the metal particles and unique sites at the metal support interface, result in enhanced deoxygenation rates to generate saturated products at atmospheric pressure. The intimacy between Pd particles and their TiO<sub>2</sub> supports for EVOH conversion is also discussed.

# 1. Introduction

The polymer industry produces more than 400 million metric tons of polymers annually and it is projected to reach 700 million metric tons by 2030. Less than 10% of the polymers are recycled, with the majority either incinerated or landfilled, which may create secondary pollutants that negatively affect the environment.<sup>2</sup> Several solutions are often implemented to recycle these discarded plastics. Among these solutions, mechanical recycling has been implemented; however, this approach brings limitations when attempting to produce highvalue products.3,4 While chemical recycling and upcycling have proven effective for some well-known polymers, different chemical strategies are often needed to regenerate high-value monomers or valuable chemicals from some of the most common streams.<sup>4-7</sup> However, implementing these approaches becomes challenging if feedstock streams contain additives or multiple resins that cannot be separated through conventional physical sorting methods.8,9

As the industry evolved, multilayered films have gained greater importance, as these multiple thin films of different polymers can better fulfill consumer needs while minimizing material utilization. However, this creates a dilemma. While the use of multilayered films leads to beneficial outcomes such as prolonged product shelf life and lower package weight, leading

smaller biomass-derived species in recent years. <sup>17,18</sup>
We propose a new strategy for the catalytic conversion of EVOH to form compatible polymer streams, as shown in Fig. 1. This strategy relies on catalytic deoxygenation through direct C–O bond scission or sequential dehydration to

effectively remove oxygen, followed by hydrogenation. The

to decreased CO<sub>2</sub> emissions associated with transportation, <sup>13</sup> the

primary drawback of these more advanced multicomponent

as poly (vinyl alcohol-co-ethylene) (EVOH), which is widely

used as an oxygen barrier for food and pharmaceutical

packaging.14 These films also involve tie layers that can

become immiscible with the other layers upon melting. In

some cases, the concentration of these polar polymers, such

as EVOH, may be very low, making extraction difficult or

economically challenging. If these low-abundance species

could be selectively converted into more compatible

components, some of these existing recycling strategies may

be employed. While selective conversion of polyols to remove

oxygen groups is in its early stages of exploration, 15,16

selective deoxygenation has been extensively studied with

Multilayered films often contain barrier film layers, such

films is that they are extremely challenging to recycle.

Pd/TiO<sub>2</sub> nanotubes

Pd/TiO<sub>2</sub> nanotubes

Pd/TiO<sub>2</sub> nanotubes

Fig. 1 Strategy for catalytic conversion of EVOH over a reducible metal support.

School of Sustainable Chemical, Biological and Materials Engineering, University of Oklahoma, Norman, OK 73019, USA. E-mail: stevencrossley@ou.edu

† Electronic supplementary information (ESI) available. See DOI: https://doi.org/ 10.1039/d4cy00404c goal is to improve compatibility with other polymers (typically polyolefins) while avoiding the cleavage of carboncarbon bonds on the polymer backbone. This approach aims to maximize the amount of compatible polymer in the recycle stream and minimize waste. Our prior efforts with monofunctional acid catalysts have illustrated the potential for selective conversion of alcohol functional groups; however, this has not yet been coupled with metals to hydrogenate resulting products and ultimately yield a polymer that is chemically similar to polyethylene. <sup>15,16</sup>

Some metals supported on reducible oxides, such as Pd/TiO2, exhibit the promise of enabling selective C-O bond scission reactions while avoiding excess C-C hydrogenolysis. 19-21 This family of catalysts is known to create highly active sites at the metal-support interface.<sup>22</sup> The addition of Pd metal clusters, which can be reduced at modest temperatures compared to most other noble metals, typically promotes hydrogen dissociation, leading to hydrogen spillover across the surface. Consequently, this process can modulate the number of exposed cations by removing lattice O groups and increasing the number of exposed sites capable of dehydration reactions.<sup>23</sup> Hydrogen spillover also modifies the density of OH groups at the surface, which is known to modify the interaction of molecules with the catalyst surface.<sup>24</sup> This could have significant implications in polymer conversion, given the importance of polymer-support interactions in modifying product distributions.

It is well known that most polymers are readily prone to diffusion limitations on most traditional microporous catalysts. 25,26 Here, TiO2 nanotubes were synthesized to mitigate these limitations since the external surface of nanotubes is effectively an inverted pore structure, offering high amounts of accessible surface area on the external surface of the nanotubes without internal diffusion restrictions accompanying most high surface area catalysts.27 A shorter diffusion path, as we envision, would occur when reactions take place directly on the external surface of a tube. This would lead to a minimization of secondary reactions along the diffusion path when compared to a highly microporous catalyst where the intrinsic attributes of the active site are often convoluted with diffusion limitations. 28-30 To improve the redox properties of TiO2 at lower temperatures, the reducible support was functionalized with Pd metal clusters. Thus, the incorporation of Pd clusters can enhance dehydration/ hydrogenation rates by the hydrogenation of products and modification of the catalytic activity of the TiO2.30 This study is intended to advance understanding of the catalytic features necessary to selectively convert polar hydroxyl groups in multicomponent films such that the barriers to recycle these materials are reduced.

# 2. Experimental

#### 2.1 Chemicals

2,5-Dimethyltetrahydrofuran (DMTHF, 96%), 2,5-hexanediol (99%), 2-hexanol (99%), γ-valerolactone (GVL, 99%), poly(vinyl

alcohol-co-ethylene) (EVOH,  $T_{\rm m}$  = 180 °C, 32 mol% ethylene), SiO<sub>2</sub> (nanopowder, 10–20 nm particle size), tetradecane (99%), Pd(NO<sub>3</sub>)<sub>2</sub>·2H<sub>2</sub>O (~40% Pd basis), and TiO<sub>2</sub> (nanopowder < 25 nm, mixture of rutile: anatase/85:15) were purchased from Sigma Aldrich. Deuterated dimethyl sulfoxide- $d_6$  (DMSO, 99.9%) was purchased from MagniSolv. Single-wall carbon nanotubes (CNTs) were purchased from SweNT. The gases were obtained from Airgas: nitrogen (N<sub>2</sub>, ultra-high purity GD 5.0) and hydrogen (H<sub>2</sub>, ultra-high purity GR 5.0 CGA 350). A gas mixture of 5% CO/He and 5% O<sub>2</sub>/He was used for CO and O<sub>2</sub> chemisorption, respectively.

#### 2.2 Polymer preparation

The polymer used in this study, EVOH, was pulverized using a Retsch Mixer Mix CryoMill with a 50 mL grinding jar, one 25 mm grinding ball with a profile of 10 minutes of precooling at 5 Hz, followed by three cycles of grinding for 10 minutes at 25 Hz, with an intermediate cooling step of 5 minutes at 5 Hz. NMR results, presented in Table S1,† indicate that the functional groups in pellet EVOH (in its purchased state) remain unchanged compared to EVOH after the cryomilling step. This polymer pretreatment was conducted to facilitate initial mixing and enhance catalyst contact for TGA studies. For the other experiments using a semi-batch reactor, EVOH was used in pellet form. NMR analysis was conducted before and after to validate that the polymer did not undergo mechanical decomposition during the cryomilling pretreatment, revealing no significant differences, as indicated in Table S1.†

### 2.3 Catalyst preparation

To synthesize  $TiO_2$  nanotubes (TNTs), 1.7 g of  $TiO_2$  was dispersed in 157 mL of NaOH 10 M solution before undergoing the hydrothermal process at 135 °C for 24 h. The resulting hydrothermal mixture was neutralized with HCl, washed multiple times with DI water, and subsequently dried at 60 °C.  $^{31}$  The resulting powder was then calcined at 350 °C for 2 h.

The incipient wetness impregnation method was employed to synthesize 2 wt% Pd over  $TiO_2$  nanotubes (Pd/TNTs), utilizing Pd( $NO_3$ )<sub>2</sub>·2H<sub>2</sub>O as a Pd precursor. A similar approach was conducted for all the supports investigated in this study (SiO<sub>2</sub>, TiO<sub>2</sub>, and CNT). After synthesis, all the catalysts were dried at 80 °C for 12 h in a vacuum oven before undergoing another calcination process at 350 °C for 2 h.

#### 2.4 Characterization

The morphology and elemental distribution of the catalysts were monitored by a field emission gun transmission electron microscope (FEG-TEM) and energy-dispersive X-ray spectroscope (EDS), respectively. The TEM images were recorded using a JEOL JEM 2010F in an ultra-high vacuum. The catalyst powder was dispersed in DI water and coated on a copper mesh before placing it in the vacuum chamber. The surface area and pore volume of the catalysts were measured using a Micromeritics ASAP 2010 instrument. The mass loss

and product formation of the dehydration and hydrogenation of EVOH over the catalysts were monitored by a Netzsch STA F1 thermogravimetric analysis (TGA) system coupled with a QMS Aeolos 403C mass spectrometer. The functional group distribution of EVOH before and after the reaction over the catalysts was characterized by proton nuclear magnetic resonance (proton NMR) using a Varian VNMRS 400 MHz NMR spectrometer.

### 2.5 Chemisorption experiments

Oxygen chemisorption experiments were conducted to quantify the number of oxygen vacancies created under reaction conditions. For this experiment, 50 mg of catalyst mass were mixed with glass beads (150 mg) and reduced for 30 minutes at 190 °C to promote oxygen vacancy formation, followed by inert gas treatment at room temperature to remove hydrogen atoms that could be present at the catalyst surface. Small doses of O2 were then introduced through the catalyst bed using a micropulse reactor at 350 °C. A similar setup was used for the CO chemisorption, which was employed to quantify the exposed Pd metal sites. The Pd/TNTs were reduced at 100 °C previous to the CO chemisorption to avoid further reduction of the support. CO pulses were subsequently introduced at room temperature to quantify the Pd metal sites.

#### 2.6 Catalytic reactions

A gas phase dehydration reaction of 2,5-hexanediol over different catalyst samples (TNTs, Pd/TNTs, Pd/TiO<sub>2</sub>, TiO<sub>2</sub>) was carried out in a fixed bed tubular reactor. A measured amount of pelletized (250-355 µm) catalyst of 20 mg mixed with glass beads packed between quartz wools in a 1/4 inch quartz reactor tube was then pretreated at 10 °C min<sup>-1</sup> to 200 °C under flowing hydrogen and held for 30 minutes to stabilize reactor for reaction temperatures at 200 °C. The hydrogen carrier gas was set at 100 ml min<sup>-1</sup>, and the feed was introduced in a mixture of 2,5-hexanediol and GVL (1:5 volume ratio) with flow rates between 0.4-0.6 mL h<sup>-1</sup>, which was controlled using syringe pumps. The reactor temperature was controlled via an attached thermocouple to the external surface of the reactor tube aligned with the center of the catalyst bed. The reactor outlet streamline was heated to 300 °C to avoid condensation of leaving species. A micro electric actuator controlled the six-port valve used to send the sample to an inline connected gas chromatograph HP 6890 GC-FID equipped with a flame ionization detector and an Agilent HP-INNOWAX ( $L \times ID \times thickness = 30 \text{ m} \times 0.32 \text{ mm} \times 0.50 \text{ }\mu\text{m}$ ) column for separation of molecules in this reaction. The rates were extrapolated to zero time on stream to rule out the role of catalyst deactivation on reaction rates.

The response factor was achieved by flowing the reactant at the desired rate through a glass beads bed to mimic the catalyst bed. These response factors are used for further data analysis, such as conversion and carbon balance. The reaction rates were obtained using eqn (1):

reaction rate 
$$(r)$$
 (1)
$$= \frac{\text{Moles of product formed}}{\text{time} \times \text{mass of catalyst}} \text{ (mol per hour gram)}$$

The product formation yields of each species were estimated by using eqn (2):

$$Yield = \frac{Moles of a product formed per hour}{Moles of 2,5-hexanediol fed per hour} (mol\%) (2)$$

The dehydration and hydrogenation of EVOH were conducted in a thermogravimetric analyzer and semi-batch reactor at 195 °C in H2. In the TGA setup, the EVOH powder and 10 wt% of the catalyst were mixed at room temperature using a vortex system to ensure thorough mixing and effective contact with the catalyst. The mixtures were transferred into crucibles in the TGA to conduct the reactions, using the temperature profiles as follows: segment 1, the temperature was raised from 30 °C to 150 °C at a ramping rate of 10 K min<sup>-1</sup> to desorb the adsorbed H<sub>2</sub>O on the surface of both EVOH and the catalyst. Segment 2 was held at 150 °C for 30 min to pretreat the catalyst under H2 gas. Subsequently, in segment 3, the temperature was increased from 150 °C to 195 °C at a ramping rate of 5 K min<sup>-1</sup>. Lastly, in segment 4, the temperature was held at 195 °C for 1 h to carry out the dehydration and hydrogenation of EVOH.

For EVOH reactions in a semi-batch reactor, the reaction was conducted in a 50 mL three-neck round bottom flask 14/20 with one neck connected to the gas line, another connected to a condenser, and the third neck was used for chemical injection. Initially, 10 mg of catalyst and 2 mL of GVL were combined at room temperature under N<sub>2</sub>, followed by the continuous introduction of H2. The mixture was heated to 150 °C for 30 min to treat the catalyst before adding 100 mg of EVOH pellets. Afterward, the mixture was heated to 195 °C and held at this temperature for 1 h to achieve the dehydration and hydrogenation of the EVOH. The EVOH and catalyst were then removed from the GVL mixture via cooling.

For proton NMR analysis, the product mixture was introduced to the DMSO NMR solvent at 80 °C, after which the polymer mixture was fully dissolved. All reaction products were also fully dissolved in DMSO after the reaction, with no observed precipitation of polymer products in the NMR solvent. Prior to the NMR analysis, an inverse recovery pulse sequence was employed to acquire the maximum spin-lattice relaxation (T1) for both the solvent (DMSO- $d_6$ ) and the polymers (EVOH and reacted EVOH). This was done to ensure that the relaxation time could be set at five times the value of T1 for accurate and quantitative measurements. In this specific sample and environment, the longest T1 observed was 0.9 s. As a result, the relaxation delay utilized for all measurements was fixed at 5 s. The spectral width was set at 6410.3 Hz, the acquisition time was 2.56 s, complex points were set to 16384, the pulse angle was set at 90 degrees, and a total of 128 scans were conducted.

# 3. Results and discussion

#### 3.1 Catalyst characterization

Fig. 2a illustrates the results of TEM analysis conducted on both TNTs and Pd/TNTs. The TNT catalyst exhibits an average inner diameter and length of about 7.1 nm and 125 nm, as shown in Fig. 2b. The presence of Pd metal clusters was verified using energy dispersive X-ray mapping of Pd/TNTs, as illustrated in Fig. 2c. SEM and EDS analysis shows similar results, Fig. S1.† The physical characteristics of the TiO<sub>2</sub> catalysts measured by N<sub>2</sub> adsorption are provided in Table 1. As a result, the surface area of TNTs (156.2 m<sup>2</sup> g<sup>-1</sup>) is around 3.5 times higher than that of TiO<sub>2</sub> (44.1 m<sup>2</sup> g<sup>-1</sup>). Thus, the unique nanotube structure can further facilitate the accessibility of a significant portion of this surface area to large polymer molecules. The surface area and pore volume of the Pd-supported catalyst were also measured, as shown in Table S2.† It is important to note that while other inert supports may have high surface areas, they lack the unique sites present in TNTs that are crucial for selective deoxygenation chemistry, which Pd alone cannot achieve.

Oxygen chemisorption was utilized as a probe molecule technique to quantify the number of oxygen vacancies formed under H2 reduction conditions. Several studies indicate that surface defects on TiO2 favor O2 dissociation, which leads to the titration of two oxygen vacancies, even at low temperatures. 32,33 Fig. 3a indicates that the incorporation of Pd metal clusters drastically increases the number of oxygen vacancies at the surface, which explains the high dehydration rate yield for Pd/TNTs. The amount of oxygen uptake over Pd catalysts was corrected by also carrying out O2 chemisorption experiments over a Pd/SiO2 catalyst and subtracting this amount of oxygen uptake per Pd atom from the Pd/TiO2 and Pd/TNTs catalysts.

Table 1 Surface area and pore volume of TiO<sub>2</sub> catalysts

Catalyst	Surface area (m² g <sup>-1</sup> )	Pore volume (cm <sup>3</sup> g <sup>-1</sup> )	Micropore volume (cm <sup>3</sup> g <sup>-1</sup> )
TiO <sub>2</sub>	44.1	0.25	0.0012
TNTs	156.2	0.72	0.0114

Utilizing CO titration, we determined the size of Pd particles and the proportion of exposed Pd atoms, as shown in Table 2. A stoichiometric ratio of 2 for Pd/CO chemisorption was considered to quantify the exposed metals. This assumption is based on the premise that COadsorbed molecules form a bridge bond with Pd atoms.<sup>34</sup> Pd/ TiO2 and Pd/TNTs exhibited a similar mean Pd particle size, with respective values of 1.5 nm and 1.3 nm.

## 3.2 Conversion of 2,5-hexanediol over Pd supported TiO<sub>2</sub> nanotubes

To gain initial insights into the capability of reducible oxide catalysts in promoting EVOH deoxygenation, we utilized 2,5-hexanediol as a model compound. 2,5-Hexanediol and its isomers have been used previously as a surrogate to understand the catalytic conversion of EVOH under conditions not corrupted by diffusion limitations. 15,16 GVL was chosen as the green solvent for the reaction of EVOH and 2,5-hexanediol because it is a stable polar solvent and can be readily derived from biomass.35,36 This model compound was tested using different catalysts and supports: SiO<sub>2</sub> (inert support), Pd/SiO<sub>2</sub> (metallic sites), Pd/CNTs (metal site on non-acid site with high surface area support), TiO2 powder, TiO<sub>2</sub> nanotubes (TNTs), Pd/TiO<sub>2</sub>, Pd/TNTs, and a physical mixture of Pd/CNTs and TNTs.

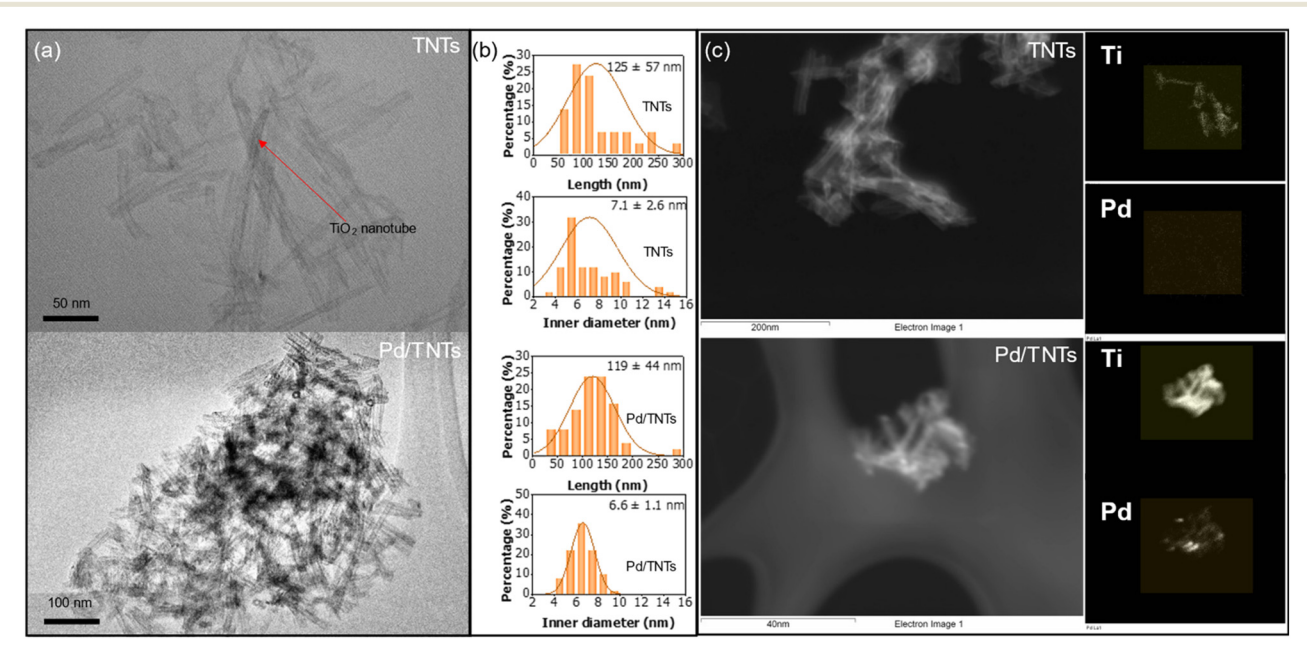


Fig. 2 (a) TEM images of TNTs and Pd/TNTs, (b) size distribution of tube inner diameter and length for TNTs and Pd/TNTs, and (c) EDS mapping of TNTs and Pd/TNTs.

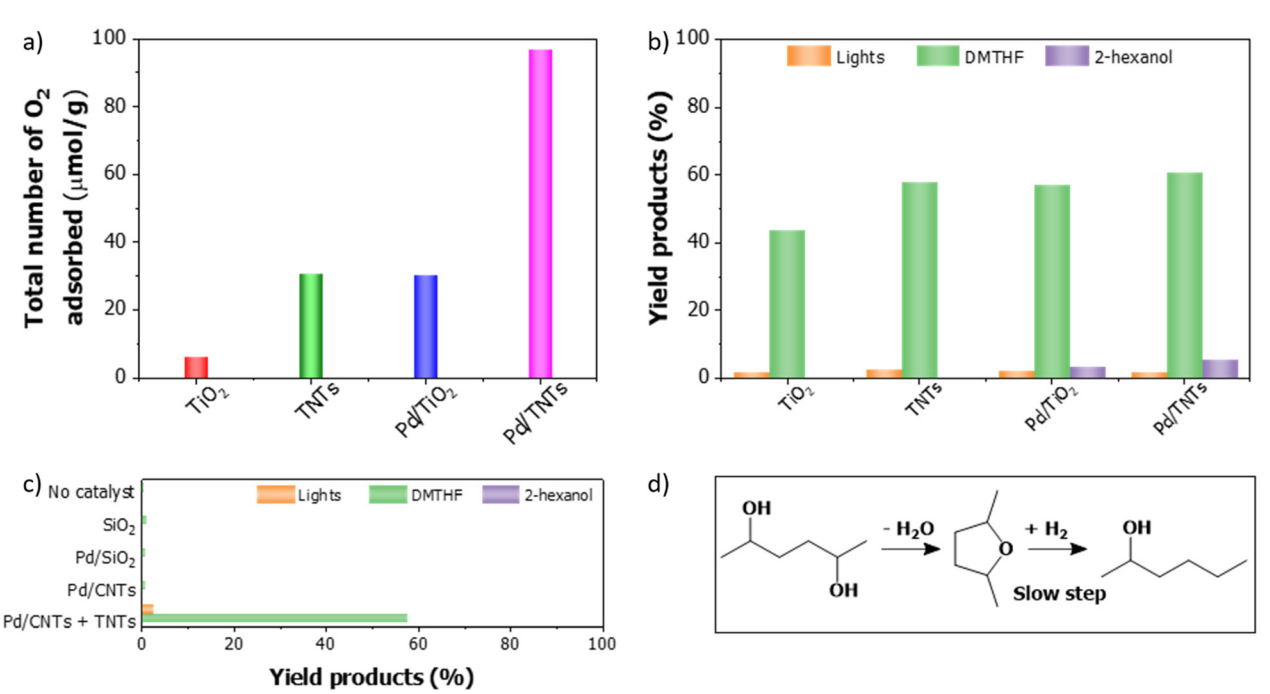


Fig. 3 (a) O<sub>2</sub> chemisorption results for TiO<sub>2</sub>, TNTs, Pd/TiO<sub>2</sub>, and Pd/TNTs. Reaction conditions: T<sub>reduction</sub> = 190 °C, T<sub>chemisorption</sub> = 350 °C, and W<sub>cat</sub> = 50 mg. (b) Yields of 2,5-hexanediol dehydration and hydrogenation over TiO<sub>2</sub>, TNTs, Pd/TiO<sub>2</sub>, and Pd/TNTs in a gas phase reactor. (c) Yields of 2,5-hexanediol dehydration and hydrogenation over SiO<sub>2</sub>, Pd/SiO<sub>2</sub>, Pd/CNTs, and Pd/CNTs + TNTs and without catalyst in a gas phase reactor. Reaction conditions for (b) and (c) are the same:  $T_{\text{reaction}} = 200 \, ^{\circ}\text{C}$ ,  $W_{\text{cat.}} = 20 \, \text{mg}$ ,  $F_{\text{H}_2} = 100 \, \text{ml min}^{-1}$ ,  $F_{\text{Feed}} = 0.6 \, \text{mL h}^{-1}$ . (d) Proposed reaction pathway. For all the cases, the feed was introduced in a mixture of 2,5-hexanediol and GVL (1:5 volume ratio). For the physical mixture of Pd/CNT + TNTs, 20 mg of Pd/CNT and 20 mg TNTs were used.

Fig. 3b illustrates the conversion of 2,5-hexanediol across different catalysts: TiO2, TNTs, Pd/TiO2, and Pd/TNTs, resulting in conversion rates of 45.4%, 60.2%, 62.2%, and 67.4%, respectively. Notably, all tested catalysts exhibit a selectivity equal to or exceeding 90% towards the primary 2,5-dimethyl tetrahydrofuran product, (DMTHF). Furthermore, as a secondary product, 2-hexanol is observed only over Pd/TiO2 and Pd/TNTs catalysts, where DMTHF undergoes an additional hydrogenation reaction, leading to the formation of saturated 2-hexanol. Thus, the abundance of DMTHF in the product distribution illustrates that the initial dehydration step is fast, followed by a slow decomposition of the ether bond under these conditions, which is aligned with observations from prior studies.<sup>15</sup> Comparable experiments were performed using inert support catalysts such as SiO<sub>2</sub>, Pd/SiO<sub>2</sub>, and Pd/CNTs. These trials demonstrated minimal

Table 2 Results of CO chemisorption studies. Values of dispersion, mean diameter, and specific surface area for Pd/TiO2 and Pd/TNTs

	$\mathrm{Pd}/\mathrm{TiO}_2$	Pd/TNTs
D (%)	73.7	82.5
$d_{\mathrm{VA}}\left(\mathrm{nm}\right)$	1.5	1.3
$S_{\rm sp} \left( {\rm m}^2 {\rm g}^{-1} \right)$	332.24	371.65
$N_{ m s}$	$5.0 \times 10^{18}$	$5.6 \times 10^{18}$
$N_{t}$	$6.8 \times 10^{18}$	$6.8 \times 10^{18}$

D: dispersion;  $d_{VA}$ : diameter;  $S_{sp}$ : specific surface area;  $N_{s}$ : total number of Pd metal atoms on the surface; Nt: total number of Pd metal atoms (surface and bulk).

conversion of 2,5-hexanediol into DMTHF or 2-hexanol. In contrast, Pd/CNTs + TNTs exhibited notable activity, primarily attributed to the Lewis acids sites located on the TNTs. These findings align with prior reports suggesting that the interface between metals and reducible supports can facilitate the hydrogenation and hydrogenolysis of C-O and C-O-C.37-39 Pd/CNTs further enhanced the activity towards lighter compounds, as illustrated in Fig. 3c.

The incorporation of Pd metal clusters directly over a reducible metal oxide introduces two additional important features. Firstly, interfacial sites at the metal/support interface are well known for their high rates of C-O bond activation. 21,22 These interfacial sites at the perimeter of the metal and TiO<sub>2</sub> support have been shown to activate said bonds due to strong O interaction with undercoordinated sites on the Ti while the connecting C is bound to the noble metal, thus enhancing C-O cleavage rates. Secondly, the presence of Pd metal clusters promotes hydrogen spillover from the metal sites to the reducible oxide support. This modifies the formation of surface OH groups and oxygen vacancies, tuning the catalytic activity of the TiO2 surface. These undercoordinated centers could also serve to dehydrate alcohols to yield olefins, which could then migrate to the metal to undergo hydrogenation. Kinetic deconvolution of these phenomena is challenging and should be a point of future studies. 19,21,40 To test the importance of sites located at the interface of Pd/TNTs, a physical mixture of TNTs and Pd/CNTs was used. Fig. 3c indicates that the absence of direct contact of Pd and TNTs does not result in the formation

of 2-hexanol, nor does it lead to a substantial increase in the yield of DMTHF. However, small yields for light products were observed for this physical mixture (Pd/CNTs + TNTs), resulting from consecutive dehydration and hydrogenation reactions of the products. Hence, these findings suggest that the ringopening chemistry of DMTHF to hexanol is likely to be predominantly facilitated via direct metal support contact, and likely promoted at the Pd/TiO2 interface. Gilkey et al. demonstrated that the conversion of 2,5-dimethylfuran (DMF) via ring-opening to 2-hexanol and 2-hexanone through ringopening chemistry is unlikely to take place on monometallic surfaces but rather occurs in bi- or multifunctional catalysts.<sup>41</sup> Our group has similarly shown that over metal supported on TiO<sub>2</sub> surfaces, for cresol conversion, <sup>21</sup> furfuraldehyde deoxygenation, 19 and furan ring opening and rearrangement, 22 the kinetically relevant active site for this selective chemistry lies at the metal/support interface.

The reaction pathway can be hypothesized, as illustrated in Fig. 3d, involving the dehydration of 2,5-hexanediol to form a cyclic ether before undergoing hydrogenation, which furthermore can undergo ring opening to yield 2-hexanol.

#### 3.3 EVOH conversion over Pd-supported TiO<sub>2</sub> nanotubes

The dehydration and hydrogenation of EVOH were also investigated via thermal gravimetric analysis (TGA) at 195 °C under a reducing environment. As shown in Fig. 4a, EVOH is thermally stable under reaction conditions in the absence of a catalyst. As a result, the addition of 2 mg TiO2 or 2 mg TNTs to 20 mg EVOH results in 0.3% and 1% mass loss, corresponding to approximately 1% and 3.4% of the total hydroxyl groups in EVOH, respectively. The mass spectra further confirmed that the weight lost under these conditions is only attributed to EVOH dehydration, leading to the generation of water as a byproduct, as is shown in Fig. S2.† Upon incorporation of Pd metal clusters over TNTs, the mass loss significantly increases to 5.7%. This indicates the removal of 18.7% of the total hydroxyl groups present in EVOH, as shown in Fig. 4b. Therefore, the incorporation of Pd on TiO2 or TNTs drastically increases the rates of dehydration. Similar studies were conducted using inert support catalysts such as SiO2 and CNT, revealing that the absence of Lewis acid

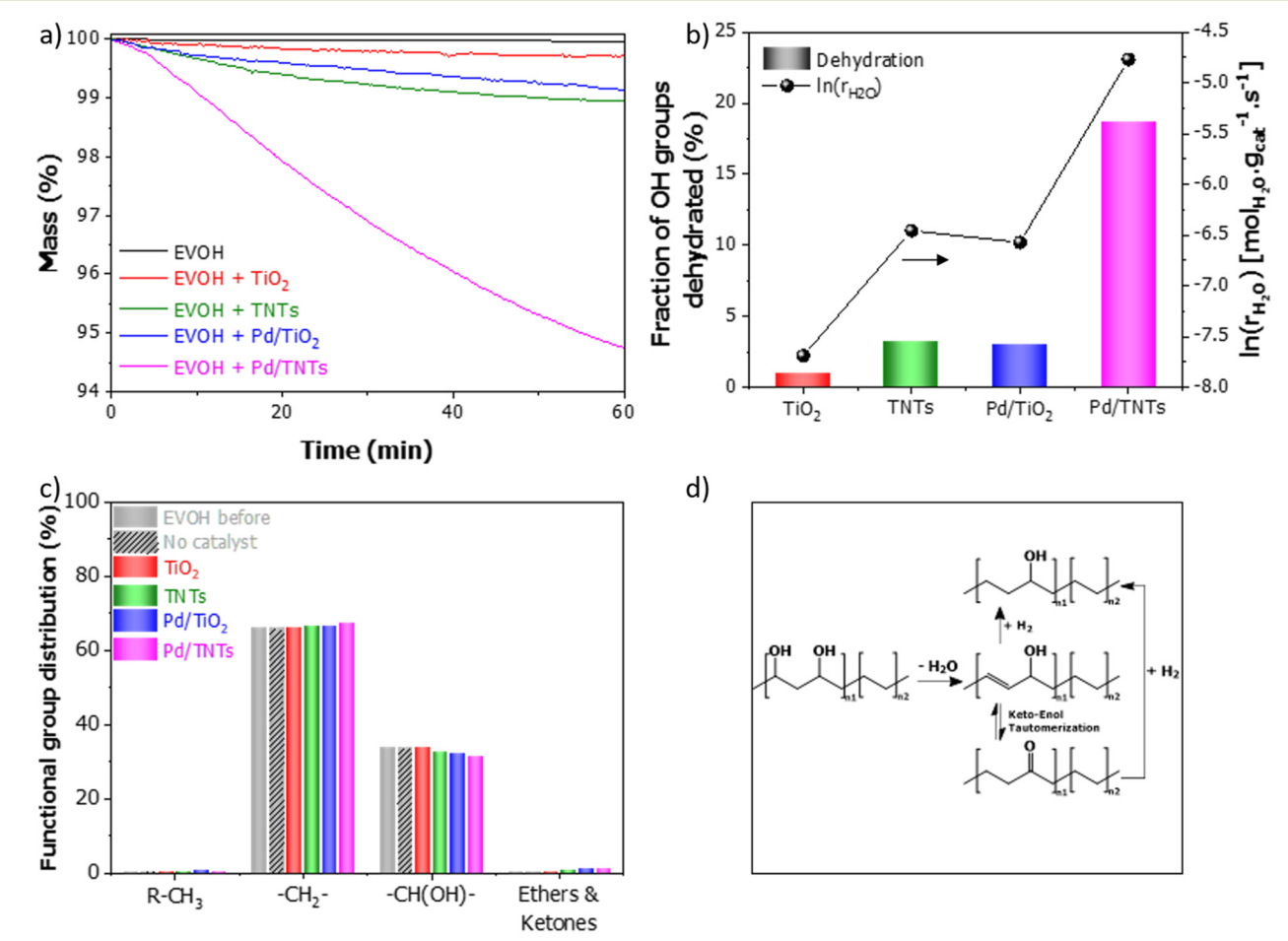


Fig. 4 (a) TGA results of dehydration and hydrogenation of EVOH over TiO2, TNTs, Pd/TiO2, and Pd/TNTs catalysts. (b) Fraction of OH groups dehydrated (%) and rate of EVOH by using TiO2, TNTs, Pd/TiO2, and Pd/TNTs as a catalyst. (c) Functional group distribution of EVOH after reaction. (d) Polymer dehydrated/hydrogenated reaction products. Reaction conditions:  $W_{\text{cat.}} = 2 \text{ mg}$ ,  $W_{\text{EVOH}} = 20 \text{ mg}$ ,  $F_{\text{H}_2} = 40 \text{ mL min}^{-1}$  and  $T_{\text{reaction}} = 195$ °C. The quantities for the functional groups related to ether and ketones were added together.

sites notably reduces the dehydration reaction of EVOH (Fig. S3†).

To further investigate the ability of the catalysts to selectively break C-O bonds, NMR analysis of the products can be seen in Fig. 4c and S4.† The number of each species was determined by considering the number of hydrogen atoms per functional group: R-CH<sub>3</sub>/3, R-CH<sub>2</sub>-R/2, R-OH/1, RCHOR (link to ether or alcohols)/1, and ketones/4. The residual oxygen species were assessed by measuring the combined H signal from the region corresponding to RCHOR (3.5-4.2 ppm) and ketones (2-2.5 ppm). The number of ketones was measured by leveraging the distinctive shift in the adjacent CH2 groups caused by this functionality (1.8-2.3 ppm). The stoichiometric number of protons associated with CH2 groups was determined by adding the summing of the primary peak of both unaffected CH2 groups (1-1.7 ppm) and the CH<sub>2</sub> groups that experienced a shift due to ketone functionality (1.8-2.3 Subsequently, the quantity of ether groups was estimated by subtracting the R-OH (4.2-4.7 ppm) from the RCHOR groups. A summary of the chemical shift ranges for the functional groups involved in the deoxygenation of EVOH is indicated in Table S3.†

The dehydration of EVOH over TiO2 and TNTs increases with the amount of residual oxygen species representing the ketones and ethers in the polymer chains, as indicated in Fig. 4c. EVOH dehydration over Pd/TNTs is followed by hydrogenation, which significantly increases the -CH<sub>2</sub>-CH<sub>2</sub>products representative of the conversion of polyvinyl alcohol (PVA) to PE-like polymers in the final products (Fig. S4†). The persistent presence of residual oxygen products indicates that further hydrogenation activity would further increase rates of PE-like products. From these results, deoxygenation of EVOH over Pd/TNTs that proceed through an initial dehydration step over the TNT surface yield dehydrated products that may undergo sequential reactions. Unsaturated products may be hydrogenated via the metal function, while the residual acid sites may facilitate ketone formation via double bond migration and keto-enol tautomerization (Fig. 4d).42 Thus given sufficient reaction time, these residual oxygen species may be further converted to saturated products over the metal function. Alternatively, if highly active sites for C-O cleavage at the metal-support interface play an important role, the direct production of saturated products via enhanced hydrogenolysis rates at the metal support interface will lead to lower yields of olefinic and ketone products.

To further study the dehydration and hydrogenation of EVOH, a semi-batch stirred reactor on a larger scale was used to improve external diffusion to the catalyst particles. The polymer reaction products were analyzed by NMR (Fig. 5a). Because GVL was used as a solvent, the residual overlapping GVL signals were subtracted from the -CH<sub>2</sub>- contribution (Fig. S5†).

EVOH conversion in a semi-batch reactor yields a similar trend in reaction products, aligning with the findings obtained with TGA analysis. TiO<sub>2</sub> and TNTs exhibit enhanced rates of OH group conversion in a well-mixed system, decreasing PVA content in the final products. However, the content of PE is similar for both catalysts, attributable to the absence of a hydrogenation function. Fig. 5a indicates that Pd/TNTs exhibit the highest deoxygenation rates. Using Pd/ TNTs as catalysts, OH groups in polymer chains significantly decreased from 33.6% to 23.7%, while the -CH<sub>2</sub>- portion increased from 65.9% to 74.4%. Thus, less residual oxygen products are observed compared to reactions conducted in TGA crucibles.

Similar studies were conducted on inert supported catalysts such as SiO2, Pd/SiO2, and Pd/CNTs. However, as shown in Fig. S6,† the results indicated that dehydration/ hydrogenation of EVOH does not occur on monometallic surfaces. In contrast, a physical mixture of Pd/CNTs and TNTs shows a slight increase in the dehydration/ hydrogenation rates. This implies that most of the deoxygenation of EVOH occurs when Pd and TiO2 or TNTs are in direct contact at sites located at the Pt/support interface as has been reported for other deoxygenation reactions, 19,22 or that dehydrated polymers diffuse along the same particle to undergo hydrogenation prior to equilibrating with the solvent phase. These results align with results observed by using 2,5-hexanediol.

The conversion can be extended to achieve higher deoxygenation rates by increasing the reaction time or catalyst loading. Fig. 5b shows the reduction of the vast majority of residual OH groups with only a minor increase in the number of CH<sub>3</sub> groups after 12 h. These results were compared with a blank reaction at 195 °C for 12 hours using the most active catalyst (10 mg of Pd/TNT), revealing no quantifiable losses in GVL solvent, as depicted in Fig. S7.† Additionally, NMR analysis of the products confirms the absence of any new peaks under these reaction conditions. Thus, this highlights the potential of this approach to convert polar functional groups while preserving the integrity of the hydrocarbon backbone.

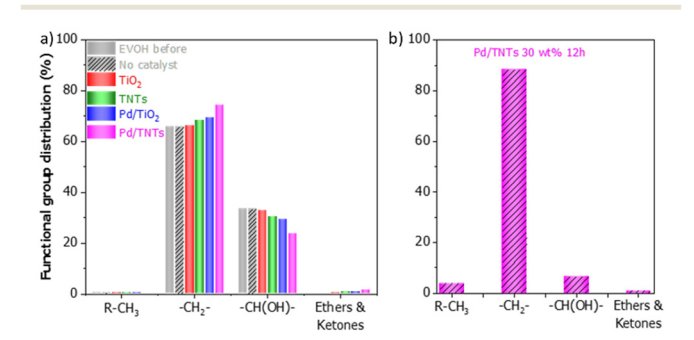


Fig. 5 Functional group distribution (%) of EVOH after reaction in a semi-batch reactor (a) after 1 h of reaction over TiO2, TNTs, Pd/TiO2, and Pd/TNTs. (b) After 12 h of reaction over Pd/TNTs. Reaction conditions: (a)  $W_{\text{cat.}} = 10 \text{ mg or (b)}$   $W_{\text{cat.}} = 30 \text{ mg}$ ;  $F_{\text{H}_2} = 60 \text{ mL min}^{-1}$ ,  $W_{\rm EVOH}$  = 100 mg,  $T_{\rm reaction}$  = 195 °C. For all the cases,  $\overset{\circ}{2}$  mL of GVL was used as a solvent. The quantities for the functional groups related to ether and ketones were added together.

# 4. Conclusions

This work shows the promise of Pd supported on TiO<sub>2</sub> nanotube (Pd/TNTs) catalysts for selective oxygen removal of polyols for both the model compound of 2,5-hexanediol as well as real EVOH streams, which is a common component of multilayered films. Our findings demonstrate that the incorporation of Pd metal clusters over TiO2 nanotubes favors hydrogen spillover in combination with an increase of Lewis acid sites, significantly enhancing dehydration/hydrogenation rates while avoiding cleavage of the polymer backbone. It is revealed that 18.5% of OH groups of EVOH are converted over Pd/TNTs, which outperforms other tested catalysts (Pd/ TiO2, Pd/SiO2, Pd/CNTs, and Pd/CNTs + TNTs). This conversion of the PVA portions of EVOH to PE-like polymers could be highly promising for improved recycling of multicomponent polymer mixtures that cannot be physically sorted.

# Data availability

The data supporting this article have been included as part of the ESI.†

# Author contributions

D-PB.: conceptualization, investigation, methodology, validation, visualization, writing - original draft. LAG: methodology, investigation, writing - review & editing. IA, LT, and ACJ: methodology, validation, writing - review & editing. HKC: methodology, writing - review & editing. LLL: conceptualization, supervision, project administration, writing - review & editing. SPC: conceptualization, supervision, project administration, funding acquisition, writing - review & editing.

# Conflicts of interest

There are no conflicts to declare.

# Acknowledgements

The authors are grateful for the financial support from the National Science Foundation under Grant No. EFRI E3P-2029394 to carry out this research. The authors acknowledge the support from the University of Oklahoma and thank Bin Wang, Kathy Wang, Jenna Holt, and Adam Feltz for the insightful discussions regarding the results.

# References

- 1 P. F. Britt, G. W. Coates and K. I. Winey, Report of the Basic Energy Sciences Roundtable on Chemical Upcycling of Polymers, U.S. Department of Energy Office of Science, 2020.
- 2 G. Celik, et al. Upcycling Single-Use Polyethylene into High-Quality Liquid Products, ACS Cent. Sci., 2019, 5, 1795-1803.
- 3 Z. O. G. Schyns and M. P. Shaver, Mechanical Recycling of Packaging Plastics: A Review, Macromol. Rapid Commun., 2021, 42, 2000415.

- 4 A. Tennakoon, et al. Catalytic upcycling of high-density polyethylene via a processive mechanism, Nat. Catal., 2020, 3, 893-901.
- 5 S. Liu, P. A. Kots, B. C. Vance, A. Danielson and D. G. Vlachos, Plastic waste to fuels by hydrocracking at mild conditions, Sci. Adv., 2021, 7, 8283-8304.
- 6 I. Vollmer, et al. Beyond Mechanical Recycling: Giving New Life to Plastic Waste, Angew. Chem., Int. Ed., 2020, 59, 15402-15423.
- 7 S. C. Kosloski-Oh, Z. A. Wood, Y. Manjarrez, J. P. De Los Rios and M. E. Fieser, Catalytic methods for chemical recycling or upcycling of commercial polymers, Mater. Horiz., 2021, 8, 1084-1129.
- 8 J. Zheng, M. Arifuzzaman, X. Tang, X. C. Chen and T. Saito, Recent development of end-of-life strategies for plastic in industry and academia: bridging their gap for future deployment, Mater. Horiz., 2023, 10, 1608-1624.
- 9 A. C. Jerdy, et al. Impact of the presence of common polymer in thermal and catalytic polyethylene decomposition, Appl. Catal., B, 2023, 325, 122348.
- 10 D. J. Walsh, E. Su and D. Guironnet, Catalytic synthesis of functionalized (polar and non-polar) polyolefin block copolymers, Chem. Sci., 2018, 9, 4703-4707.
- 11 J. R. Wagner, Multilayer Flexible Packaging, 2nd edn, 2016.
- 12 T. W. Walker, et al. Recycling of multilayer plastic packaging materials by solvent-targeted recovery and precipitation, Sci. Adv., 2020, 6, eaba7599.
- 13 E. Pauer, M. Tacker, V. Gabriel and V. Krauter, Sustainability of flexible multilayer packaging: Environmental impacts and recyclability of packaging for bacon in block, Clean. Environ. Syst., 2020, 1, 100001.
- 14 V. Muriel-Galet, G. López-Carballo, R. Gavara and P. Hernández-Muñoz, Antimicrobial Properties of Ethylene Vinyl Alcohol/Epsilon-Polylysine Films and Their Application in Surimi Preservation, Food Bioprocess Technol., 2014, 7, 3548-3559.
- 15 H. K. Chau, et al. Role of Water on Zeolite-Catalyzed Dehydration of Polyalcohols and EVOH Polymer, ACS Catal., 2023, 13, 1503-1512.
- 16 Q. P. Nguyen, H. K. Chau, L. Lobban, S. Crossley and B. Wang, Mechanistic insights into the conversion of polyalcohols over Brønsted acid sites, Catal. Sci. Technol., 2023, 13, 4477-4488.
- 17 T. Omotoso, S. Boonyasuwat and S. P. Crossley, Understanding the role of TiO2 crystal structure on the enhanced activity and stability of Ru/TiO2 catalysts for the conversion of lignin-derived oxygenates, Green Chem., 2014, 16, 645-652.
- 18 S. Boonyasuwat, T. Omotoso, D. E. Resasco and S. P. Crossley, Conversion of guaiacol over supported Ru catalysts, Catal. Lett., 2013, 143, 783-791.
- 19 N. M. Briggs, et al. Identification of active sites on supported metal catalysts with carbon nanotube hydrogen highways, Nat. Commun., 2018, 9, 3827.
- 20 L. D. Ellis, J. Ballesteros-Soberanas, D. K. Schwartz and J. W. Medlin, Effects of metal oxide surface doping with

- phosphonic acid monolayers on alcohol dehydration activity and selectivity, Appl. Catal., A, 2019, 571, 102-106.
- 21 T. O. Omotoso, B. Baek, L. C. Grabow and S. P. Crossley, Experimental and First-Principles Evidence for Interfacial Activity of Ru/TiO2 for the Direct Conversion of m-Cresol to Toluene, ChemCatChem, 2017, 9, 2642-2651.
- 22 T. Omotoso, et al. Stabilization of furanics to cyclic ketone building blocks in the vapor phase, Appl. Catal., B, 2019, 254, 491-499.
- 23 R. Prins, Hydrogen spillover. Facts and fiction, Chem. Rev., 2012, 112, 2714-2738.
- 24 L. A. Gomez, et al. Selective Reduction of Carboxylic Acids to Aldehydes with Promoted MoO3 Catalysts, ACS Catal., 2022, 12, 6313-6324.
- 25 I. Vollmer, M. J. F. Jenks, R. Mayorga González, F. Meirer and B. M. Weckhuysen, Plastic Waste Conversion over a Refinery Waste Catalyst, Angew. Chem., 2021, 60, 16101–16108.
- 26 A. C. Jerdy, et al. Deconvoluting the roles of polyolefin branching and unsaturation on depolymerization reactions over acid catalysts, Appl. Catal., B, 2023, 337, 122986.
- 27 S. Crossley, J. Faria, M. Shen and D. E. Resasco, Solid nanoparticles that catalyze biofuel upgrade reactions at the water/oil interface, Science, 2010, 327, 68-72.
- 28 S. P. Crossley, D. E. Resasco and G. L. Haller, Clarifying the multiple roles of confinement in zeolites: From stabilization of transition states to modification of internal diffusion rates, J. Catal., 2019, 372, 382-387.
- 29 R. J. Gorte and S. P. Crossley, A perspective on catalysis in solid acids, J. Catal., 2019, 375, 524-530.
- T. Hengsawad, T. Jindarat, D. E. Resasco and S. Jongpatiwut, Synergistic effect of oxygen vacancies and highly dispersed Pd nanoparticles over Pd-loaded TiO2 prepared by a singlestep sol-gel process for deoxygenation of triglycerides, Appl. Catal., A, 2018, 566, 74-86.
- 31 V. V. Pham, et al. Photoreduction route for Cu<sub>2</sub>O/TiO<sub>2</sub> nanotubes junction for enhanced photocatalytic activity, RSC Adv., 2018, 8, 12420-12427.

- 32 S. Wendt, et al. Oxygen vacancies on TiO<sub>2</sub>(110) and their interaction with H2O and O2: A combined high-resolution STM and DFT study, Surf. Sci., 2005, 598, 226-245.
- 33 U. Diebold, The surface science of titanium dioxide, Surf. Sci. Rep., 2003, 48, 53-229.
- 34 P. Canton, et al. Pd/CO average chemisorption stoichiometry in highly dispersed supported Pd/γ-Al<sub>2</sub>O<sub>3</sub> catalysts, Langmuir, 2002. 18, 6530-6535.
- 35 G. W. Huber and A. Corma, Synergies between bio- and oil refineries for the production of fuels from biomass, Angew. Chem., Int. Ed., 2007, 46, 7184-7201.
- F. Kerkel, M. Markiewicz, S. Stolte, E. Müller and W. Kunz, The green platform molecule gamma-valerolactone biodegradability, solvent properties, potential applications, Green Chem., 2021, 23, 2962-2976.
- 37 D. Sun, et al. Production of C4 and C5 alcohols from biomass-derived materials, Green Chem., 2579-2597.
- 38 K. Tomishige, Y. Nakagawa and M. Tamura, Design of supported metal catalysts modified with metal oxides for hydrodeoxygenation of biomass-related molecules, Curr. Opin. Green Sustainable Chem., 2020, 22, 13-21.
- 39 S. Kim, et al. Recent advances in hydrodeoxygenation of biomass-derived oxygenates over heterogeneous catalysts, Green Chem., 2019, 21, 3715-3743.
- 40 L. A. Gomez, C. Q. Bavlnka, T. E. Zhang, D. E. Resasco and S. P. Crossley, Revealing the Mechanistic Details for the Selective Deoxygenation of Carboxylic Acids over Dynamic MoO<sub>3</sub> Catalysts, ACS Catal., 2023, 13, 8455-8466.
- 41 M. J. Gilkey, A. V. Mironenko, L. Yang, D. G. Vlachos and B. Xu, Insights into the Ring-Opening of Biomass-Derived Furanics over Carbon-Supported Ruthenium, ChemSusChem, 2016, 9, 3113-3121.
- 42 S. Attia, M. C. Schmidt, C. Schröder and S. Schauermann, Formation and Stabilization Mechanisms of Enols on Pt through Multiple Hydrogen Bonding, ACS Catal., 2019, 9, 6882-6889.